BIOCHEMISTRY
including biophysical chemistry & molecular biology

Article

pubs.acs.org/biochemistry

Femtosecond Photodynamics of the Red/Green Cyanobacteriochrome NpR6012g4 from *Nostoc punctiforme*. 1. Forward Dynamics

Peter W. Kim,[†] Lucy H. Freer,[†] Nathan C. Rockwell,[‡] Shelley S. Martin,[‡] J. Clark Lagarias,[‡] and Delmar S. Larsen*,[†]

[†]Department of Chemistry and [‡]Department of Molecular and Cell Biology, University of California, One Shields Avenue, Davis, California 95616, United States

Supporting Information

ABSTRACT: Phytochromes are well-known red/far-red photosensory proteins that utilize the photoisomerization of a linear tetrapyrrole (bilin) chromophore to detect the ratio of red to far-red light. Cyanobacteriochromes (CBCRs) are related photosensory proteins with a bilin-binding GAF domain, but much more diverse spectral sensitivity, with five recognized subfamilies of CBCRs described to date. The mechanisms that underlie this spectral diversity have not yet been fully elucidated. One of the main CBCR subfamilies photoconverts between a red-absorbing ground state, like the familiar P_r state of phytochromes, and a green-absorbing photoproduct (P_g). Here, we examine the ultrafast forward photodynamics of the red/green CBCR NpR6012g4 from the *NpR6012* locus of the nitrogen-fixing cyanobacterium *Nostoc punctiforme*. Using transient absorption spectroscopy with broadband detection and multicomponent global analysis, we observed multiphasic excited-state dynamics that induces the forward reaction (red-absorbing to green-absorbing), which we interpret as arising from ground-state heterogeneity. Excited-state decays with lifetimes of 55 and 345 ps generate the primary photoproduct (Lumi-R), and the fastest decay (5 ps) did not produce Lumi-R. Although the photoinduced kinetics of Npr6012g4 is comparable with that of the Cph1 phytochrome isolated from *Synechocystis* cyanobacteria, NpR6012g4 exhibits a ≥2−3-fold higher photochemical quantum yield. Understanding the structural basis of this enhanced quantum yield may prove to be useful in increasing the photochemical efficiency of other bilin-based photosensors.

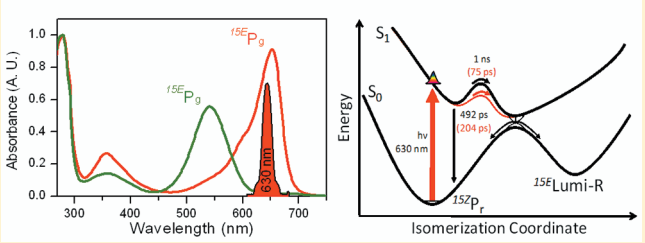

Photosensory proteins play important roles in the photobiology of both photosynthetic and nonphotosynthetic organisms.[1−5] They can also serve as powerful tools in fluorescent probe development and in the emerging field of optogenetics.[6−11] The red light-sensing phytochromes, critical regulators of photomorphogenesis in higher plants, hold considerable promise for biomedical research because of the greater tissue penetration of red or near-infrared light into mammalian tissue.[7] Phytochromes utilize linear tetrapyrrole (bilin) chromophores (Figure 1A) to reversibly photoconvert between red-absorbing P_r and far red-absorbing P_{fr} states, with primary photochemistry generally thought to occur at the 15,16 double bond.[12−14] The bilin chromophore is bound within a conserved pocket on a GAF (cGMP phosphodiesterase/adenylyl cyclase/FhlA) domain that is part of a conserved photochemical core module consisting of PAS, GAF, and PHY domains.[1,15−20]

Recently, a new family of cyanobacterial phytochrome relatives was discovered; these cyanobacteriochromes (CBCRs) require only the GAF domain itself to assemble with the chromophore and undergo photoswitching activity. CBCRs utilize phycocyanobilin (PCB) as their chromophore and exist in several subfamilies with considerable variation in their spectral photosensory activity.[9,21−33] One of the main subfamilies, the red/green CBCRs, exhibits a red-absorbing *15Z* ground state ($^{15Z}P_r$) and photoconverts to a green-absorbing *15E* photoproduct ($^{15E}P_g$), which can thermally revert to P_r over time (Figure 1A).[9,26,28,30]

The first red/green CBCR to be described was GAF2 of the protein encoded by the locus *all1069* from *Nostoc* sp. PCC7120 (AnPixJg2), characterized by Ikeuchi and colleagues.[26] AnPixJ possesses two other bilin-binding GAF domains (i.e., GAF3 and GAF4), neither of which exhibits photoactivity despite the high level of sequence identity of each to AnPixJg2 (Figure S1 of the Supporting Information). Prediction of photobiological function is therefore challenging for these proteins, because there is no obvious difference between an active photosensor and an inert bilin-binding protein at the level of amino acid sequence. This poses a challenge for attempts to infer function or to use such proteins in engineering efforts. Indeed, the number of CBCR sequences found in genome sequencing projects greatly exceeds the number whose behavior has been experimentally verified. Examination of the detailed photochemical behavior of

Received: September 27, 2011
Revised: December 1, 2011
Published: December 12, 2011

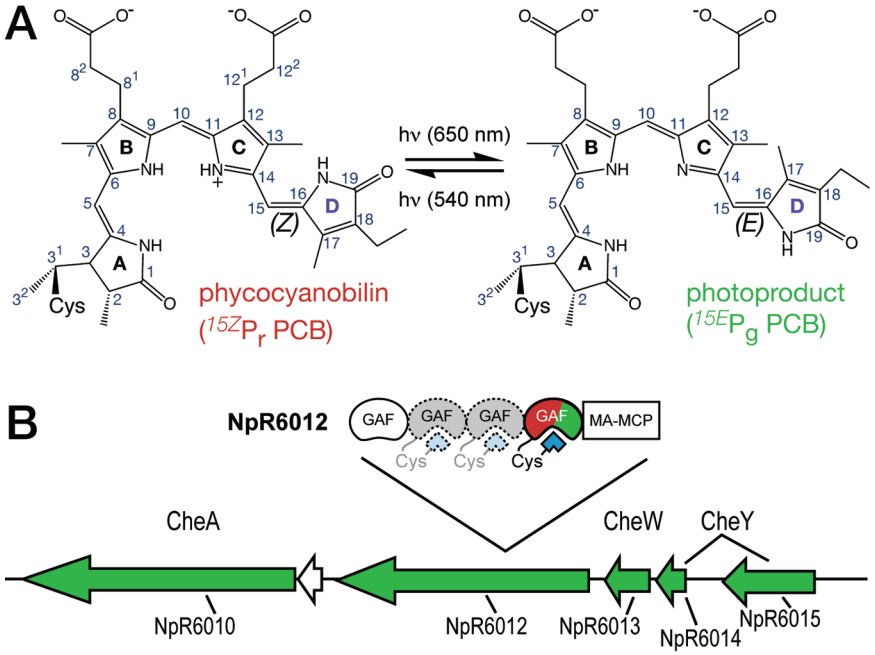

Figure 1. Proposed photostates of the red/green CBCR NpR6012g4. (A) As a working model, we follow a recent report[30] that suggested that the phycocyanobilin chromophore is protonated in the red-absorbing $^{15Z}P_r$ state (left) but deprotonated in the green-absorbing $^{15E}P_g$ state (right; protonated B-ring tautomer shown). (B) The context of the *NpR6012* locus within the *Nostoc punctiforme* chromosome is shown; neighboring open reading frames encode other components of two-component taxis systems. The domain structure of the NpR6012 protein is shown. The most N-terminal GAF domain (GAF1) lacks a conserved Cys residue required for bilin binding, while GAF2 and GAF3 are also putative red/green CBCRs. Complete dark reversion of P_g to P_r takes >20 hours.

red/green CBCRs is thus an important step in elucidating the differences between active and inactive examples. While the nanosecond-transient fluorescence photodynamics of AnPixJ has recently been described,[30] the femtosecond characterization of the primary photodynamics of red/green CBCRs has not yet been reported. Such rapid kinetic measurements can be combined with broadband detection and global data analysis[34,35] to provide a useful probe of the excited-state behavior of photoproteins.[36−43] This information should prove to be useful in elucidating the differences between active and inert red/green CBCRs and in understanding the mechanisms that generate the diverse photocycles of CBCRs compared to canonical phytochromes.

The cyanobacterium *Nostoc punctiforme* ATCC 29133, which is closely related to *Nostoc* sp. PCC7120, possesses an apparent ortholog to AnPixJ, NpR6012 (NpPixJ in ref 26), that encodes a protein with four GAF domains and a methyl chemotaxis output domain (Figure 1B). However, unlike the fourth domain of ANPixJ, the fourth bilin-binding GAF domain of NpR6012 (Figure S1 of the Supporting Information), NpR6012g4, exhibits a robust red/green photocycle. Our study probes the femtosecond photodynamics of the forward photoconversion ($^{15Z}P_r$ to $^{15E}P_g$) using broadband detection in the visible range of the spectrum and global analysis. NpR6012g4 exhibits multiexponential excited-state time scales, reflecting ground-state heterogeneity, two of which decay to a Lumi-R photoproduct similar to that of AnPixJ.[26,30] Compared to red/far-red phytochromes,[36,38,44] NpR6012g4 exhibits an unusually high quantum yield of approximately 32%. This work thus provides new insight into the ultrafast photochemical behavior of red/green CBCRs that contrasts with the analogous conversion in traditional red/far-red switching phytochromes.

MATERIALS AND METHODS

Purification and Characterization of NpR6012g4. Multiple-sequence alignment of GAF domains of NpR6012 (NpPixJ) and AnPixJ was performed using MUSCLE.[45] A DNA region encoding NpR6012g4 (amino acids 585−760 of the *NpR6012* locus) was amplified by polymerase chain reaction from *N. punctiforme* genomic DNA (gift of E. L. Campbell and J. C. Meeks, University of California, Davis, CA) using appropriate primers, followed by cloning into the unique *Nco*I and *Sma*I sites of pBAD-Cph1-CBD.[46] Coexpression with PCB biosynthetic machinery in *Escherichia coli* followed a published procedure,[47] and purification of GAF domains as intein−chitin binding domain (intein−CBD) fusions followed the procedure employed for *Synechocystis* Cph1.[46] After lysis, ultracentrifugation, and binding to chitin resin (NEB) in accordance with the manufacturer's instructions, intein cleavage was initiated by addition of DTT to the column, followed by overnight incubation at 4 °C. Peak fractions were pooled and dialyzed against TKKG buffer [25 mM TES-KOH (pH 7.8), 100 mM KCl, and 10% (v/v) glycerol] overnight prior to being frozen in liquid nitrogen and stored at −80 °C. Absorbance spectra were recorded at 25 °C on a Cary 50 instrument modified to allow top-down illumination of the sample to initiate photochemistry, and denaturation assays were performed using 6 M guanidinium chloride, 100 mM citric acid (pH 2.2).[32,48] Circular dichroism (CD) spectra were recorded at 25 °C on an Applied Photophysics Chirascan instrument using a 2 nm bandwidth and are reported as baseline-corrected single scans without smoothing. Photochemical difference spectra are reported as 15*Z* (dark) minus 15*E* (red irradiated).[32]

dx.doi.org/10.1021/bi201507k | *Biochemistry* 2012, 51, 608−618

Transient Signals. The dispersed-probe transient absorption setup was constructed from an amplified Ti:sapphire laser system (Spectra Physics Spitfire Pro + Tsunami) operating at 1 kHz, which produced 2.25 mJ pulses of 800 nm fundamental output with a 40 fs (full width at half-maximum) duration.[49] The 800 nm fundamental pulse train from the amplifier was split into multiple paths. One path generated the dispersed white-light probe continuum (440−750 nm) by focusing the laser pulses into a slowly translating CaF_2 crystal. A second path was used to generate the tunable visible pulse from a home-built noncollinear optical parametric amplifier (NOPA) as an excitation/pump source, which was tuned to be resonant with the visible absorption spectrum for the transient absorption measurements (Figure 2A). The pump beam was chopped at 500 Hz to generate difference spectra with respect to the non-pumped ground-state spectrum. The probe beam was optically delayed with respect to the pump pulse by a computer-controlled linear-motor stage (Newport IMS 6001), which allowed a temporal separation of up to 7 ns. Pump pulses were linearly polarized at 54.7° (magic angle) with respect to probe pulses. Pump pulse spot diameters of 250−360 μm and the broadband probe pulses were focused to ~50 μm as estimated using a micrometer stage and razor blade. The appreciably greater pump pulse volume minimizes artifactual contributions to the signals because of varying spatial overlap between pump and probe beams and was confirmed by monitoring the signal amplitude and spectral shape while dithering the pump beam with respect to the probe beam.

The temporal resolution of the experiment was estimated to be 100 fs using the rise time of the excited-state absorption bands. The sample was flowed continuously (~30 mL/min) in a closed circuit to ensure fresh sample for each excitation pulse. Before protein entered the cuvette, it was continuously illuminated with ~2 mW of green LED light (Epitex Inc., model L525-66-60) through a quartz window to keep the sample in the P_r state during the ultrafast experiment. The path length of the quartz cuvette was 2 mm, and the optical density at the red absorbance band was 0.3−0.4 at that path length. All experiments were conducted at room temperature (20 °C).

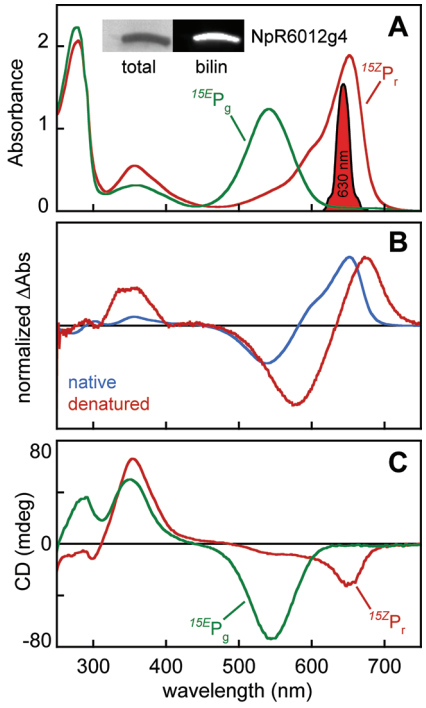

Figure 2. Optical properties of NpR6012g4. (A) Absorption spectra are shown for NpR6012g4 in the $^{15Z}P_r$ (red) and $^{15E}P_g$ (green) states. The laser spectrum of the 630 nm pump pulse is colored red. In the inset, the total protein (left) and covalently bound bilin (right) are shown for purified NpR6012g4. (B) Normalized photochemical difference spectra are shown for native NpR6012g4 (blue) and NpR6012g4 denatured in acidic guanidinium chloride (red). Peak wavelengths of 677 and 580 nm are consistent with a covalent PCB adduct as observed for AnPixJ.[26] (C) Circular dichroism spectra are shown for NpR6012g4 in the $^{15Z}P_r$ (red) and $^{15E}P_g$ (green) states.

RESULTS

NpR6012g4 Is a Red/Green CBCR. NpR6012g4 was cloned into an intein−CBD expression system and expressed in *E. coli* engineered to produce PCB. The purified protein possesses a covalently bound bilin and exhibited robust red/green photoconversion with essentially 100% switching efficiency between P_r and P_g populations (Figure 2A). Denaturation analysis confirmed the presence of a covalent PCB adduct (Figure 2B), similar to that observed for AnPixJ.[26] Examination of the NpR6012g4 photocycle by circular dichroism (CD) spectroscopy demonstrated that the long-wavelength transitions of both the red-absorbing P_r and green-absorbing P_g states exhibited negative CD (Figure 2C). This is similar to the behavior of dual-Cys CBCRs and to bacteriophytochromes with biliverdin chromophores, but differs from that of cyanobacterial and plant phytochromes that use PCB or phytochromobilin chromophores.[27,32,46,50] These results demonstrate that NpR6012g4 is a functional red/green CBCR and an excellent candidate for examination of the red/green photocycle by ultrafast spectroscopic techniques.

The transient absorption difference spectra at select delay times are contrasted in Figure 3, and four overlapping

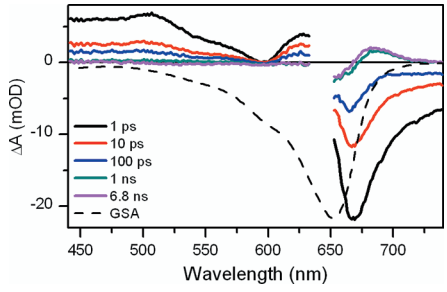

Figure 3. Transient difference spectra for the $^{15Z}P_r \rightarrow {}^{15E}$Lumi-R forward reaction at selected probe times (specified in the inset) overlaid with the inverted ground-state absorption spectra of the $^{15Z}P_r$ state (GSA, dashed line).

contributions can be discerned: (1) a negative bleach signal that originates from the loss of ground-state absorption (GSA) and matches the inverted absorption spectrum, (2) a negative stimulated emission (SE) signal that originates from the photo-induced radiative decay of the excited state, peaking at approximately 660 nm, (3) broad positive excited-state absorption (ESA) bands from $S_1 \rightarrow S_n$ transitions, and (4) a positive Lumi-R photoproduct band at later times, peaking at approximately 680 nm. The SE and ESA bands are only observed when the PCB chromophore is in the excited state (P_r*). These are

well-separated from the bleach and Lumi-R bands. Hence, at any probe time, residual P_r* can be confirmed by the observation of these bands. The 1 ps transient spectrum (Figure 3, solid black line) exhibits a strong negative band centered at 670 nm and a broad positive ESA band from 440 to 625 nm. A depression in the ESA at 590 nm corresponds to the vibronic band of the P_r GSA previously observed in *Synechocystis* Cph1.[51] The strong negative band at 670 nm at early times (<100 ps) that is red-shifted with respect to the GSA (dashed line) corresponds to the overlapping SE, which extends to the red (>740 nm). The blue side of the bleach (<650 nm) is dominated by the strongly overlapping ESA at early times, which results in no discernible negative bleach signal. At later times, the GSA bleach is partially offset by Lumi-R absorbance at 680 nm.

As the spectrum evolves over time, the excited-state markers (ESA and SE bands) decay and the appearance of the primary ground-state photoproduct (Lumi-R absorption at 680 nm) is observed. This evolution is completed within 1 ns, and Lumi-R persists beyond the 7 ns delay time range of the experiment. The evolution of the P_r* population into Lumi-R is more readily visualized in kinetic traces at individual wavelengths (Figure 4).

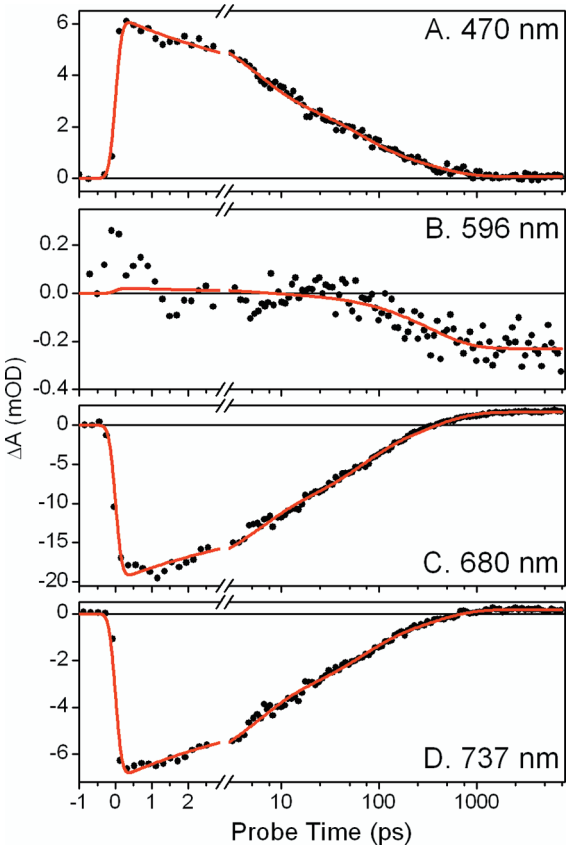

Figure 4. Kinetic traces of the forward reaction at selected probe wavelengths of (A) 470, (B) 596, (C) 680, and (D) 737 nm. The kinetic traces are fitted with the target model (red line in Figure 6A).

The ESA (Figure 4A) and SE (Figure 4D) signatures of P_r* decay with identical kinetics with multiple time scales. The formation of Lumi-R can be resolved at 680 nm (Figure 4C) as the SE undergoes a transition to the Lumi-R photoproduct absorption. To understand and characterize the observed multiphasic relaxation kinetics, we developed a target model (solid red lines) to fit the data to a set of microscopic population-to-population kinetics.

Global Analysis. In lieu of analyzing individual kinetic traces, we analyzed the multiwavelength dynamics within the global analysis formalism.[34,35] This approach fits the data to an underlying postulated multipopulation "target" model and estimates the concentration profiles and species-associated difference spectra (SADS) of the constituent populations. This is accomplished by fitting the data with numerical solutions of linear first-order differential equations describing a postulated model (eq 1):

$$\frac{dn_i}{dt} = A_i I(t) + \sum_j K_{ij} n_j \quad (1)$$

where n_i represents the microscopic population of interest, $A_i I(t)$ is the pump pulse width over time, and K_{ij} is the rate constant matrix describing the exponential flow from one population into another. If the underlying target model accurately describes the dynamics, then the extracted spectra for the populations are SADS and represent the true difference spectra of the constituent populations. If inaccurate, the resulting spectra are evolutionarily associated difference spectra (EADS) and are combinations of the underlying SADS, but such EADS can still be used to interpret the data, although from a weakened perspective.[34,35] The integrated solutions to the linear differential equations in eq 1 are an ensemble of single exponentials, which is appropriate for first-order processes commonly observed in primary femtosecond photochemical reactions.

In constructing the appropriate target model to interpret the measured data, we first used a simpler approach, whereby a sequential model of multiple states is used to fit the full data set and estimate the underlying "apparent" (i.e., directly observed) time scales in the data. The EADS from such an analysis are the averaged spectral signatures of states with increasing lifetimes (Figure 5A). Although this "sequential EADS" approach does describe the data, it does not decompose these apparent time scales into the microscopic rate constants describing one microscopic population evolving from one state into another, which requires a more sophisticated target model analysis. The sequential EADS are nevertheless useful in extracting the spectral evolution of the reaction and its apparent time scales, as demonstrated below, and in construction and validation of specific target models.

A four-compartment sequential model (Figure 5A) is sufficient to describe the measured forward reaction data over the entire spectral and temporal range. The estimated time constants from the sequential EADS approach are 5, 54, and 360 ps and a nondecaying (i.e., ∞) component and are similar to time scales observed in previous ultrafast studies of *Synechocystis* Cph1 (3, 14−30, and 134 ps time scales).[38,40,43] The estimated EADS of this four-component sequential model (Figure 5B) share similar spectral characteristics with the raw transient spectra (Figure 3), with the first three EADS (EADS1−EADS3) exhibiting ESA and SE excited-state features. This indicates that a P_r* population persists to longer times. In contrast to EADS1−EADS3, the final spectrum (EADS4) is a clean difference spectrum for the Lumi-R population, with no discernible P_r* contributions. To confirm that these EADS are constructed from linear combinations of P_r* and Lumi-R populations, we subtracted the P_r* contribution from each EADS by normalizing each spectrum (EASD1−EADS3) to the ESA band from 440 to 500 nm (Figure 5C). Because both Lumi-R and bleach (estimated from the GSA,

dx.doi.org/10.1021/bi201507k | *Biochemistry* 2012, 51, 608−618

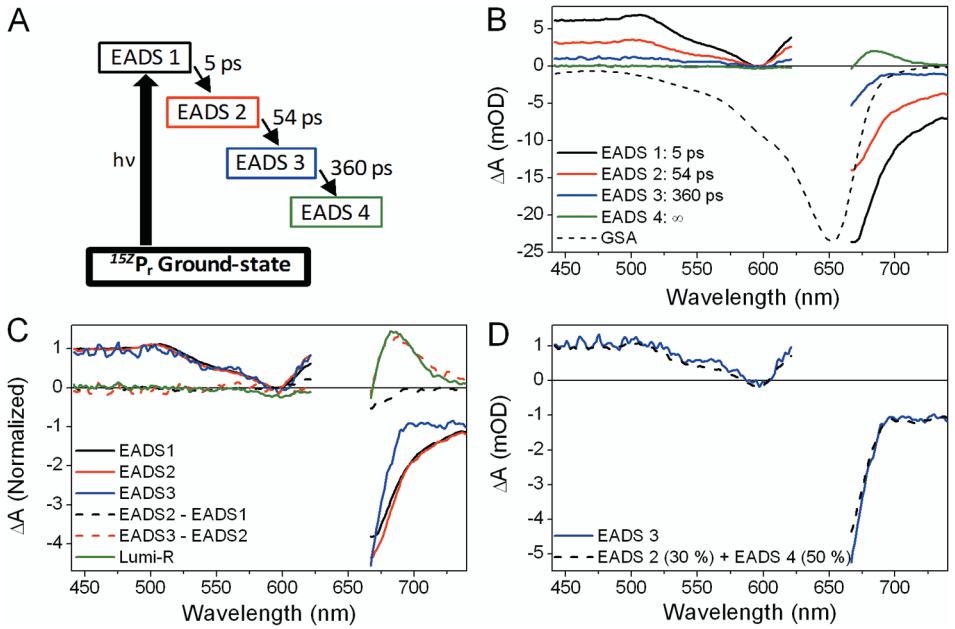

Figure 5. Spectral analysis based on a four-component sequential model. (A) Schematic of the sequential model with associated time constants for each state. (B) EADS overlaid with P_r-inverted GSA (dashed line). Colors are from panel A. (C) EADS1, -2, and -3 (black, red, and blue, respectively) normalized at the ESA band (420−500 nm). Subtraction of the normalized EADS1 from EADS2 (cyan) and EADS2 from EADS3 (magenta) demonstrates spectral evolution that is independent of excited-state decay. The Lumi-R spectrum (green) is overlaid for comparison and overlaps with the normalized EADS3 minus EADS2 difference spectrum. (D) Decomposition of the EADS3 spectrum as a linear combination of EADS2 and EADS4.

dashed line) bands negligibly contribute at these wavelengths, this normalization scales each EADS to the same contribution of P_r*. This assumes that the relative amplitude of ESA is strictly correlated with P_r* (the spectrum does not demonstrate appreciable spectral changes in time as demonstrated below). Normalized EADS1 and EADS2 are spectrally nearly identical (Figure 5C, black and red curves, respectively), indicating that the during the 5 ps decay, no spectral change in the transient absorption data occurs. Consequently, this phase of evolution in the data does not generate a Lumi-R population in any measurable amount and represents only the decay of part of the excited-state P_r* population. In contrast, normalized EADS3 (Figure 5C, blue curve) differs from EADS1 and EADS2 with a difference (dashed red curve) that perfectly overlaps with the Lumi-R EADS (green curve). EADS3 can be decomposed into a nearly perfect superposition of EADS2 (or EADS1) and EADS4 (i.e., Lumi-R) (Figure 5D), indicating that Lumi-R is formed only on the 54 and 360 ps time scales and not on the 5 ps time scale.

This decomposition demonstrates that only two time-dependent populations (P_r* and Lumi-R) with fixed spectra are needed in the target analysis to describe the measured transient data. Furthermore, this validates the assumption that the P_r* spectrum is unchanging and also established that only three exponentials are required to fit the data, implying the presence of at least three populations (i.e., compartments or distinct states). These three populations could arise via ground-state heterogeneity, bifurcation of the excited-state surface to yield multiple P_r* populations, or both. Because of the observed ground-state heterogeneity of the $^{15E}P_g$ "reverse" photodynamics (manuscript in preparation, DOI: http://dx.doi.org/10.1021/bi2017365), we favor the simple interpretation that the $^{15Z}P_r$ ground state is also heterogeneous, although more complicated models were also tested against the data (Figure S2 of the Supporting Information). An inhomogeneous target model that best explained the data consisted of three ground-state P_r populations (GS1−GS3), with only GS2 and GS3 generating the Lumi-R photoproduct (Figure 6A). The resulting P_r* SADS for each ground-state population are nearly identical, and their respective amplitudes in the transient signals result from variation of only the occupancy of each ground-state population. This model fits the data well (Figure 4, solid lines) and produces the SADS for the three excited-state intermediates shown in Figure 6B, with the time constants listed in Table 1. The estimated concentration profiles for the underlying populations are shown in Figure 6C and are color-coded to the other two panels. The final concentration of the primary photoproduct, Lumi-R (Figure 6C, green line), shows that the Φ of the primary photoreaction is 32%.

In final target model, the first excited-state intermediate 1 (ESI1) is photogenerated from GS1 and exhibits a fast 5 ps decay back to GSI without forming any Lumi-R. In contrast, ESI2 and ESI3 are simultaneously photogenerated from GS2 and GS3, respectively, and do generate Lumi-R. The non-productive population from each ESI is assumed to decay back into the respective ground-state population (although this cannot be confirmed from the data alone). The amplitude and spectral shape of the three ESI SADS are nearly identical (Figure 6B), with clear excited-state ESA and SE contributions, despite no attempt to constrain such a result during the fitting procedure. Interestingly, the ESI SADS have slightly different amplitudes at approximately 600 nm, which suggests either that there is some structural deformation in the excited state (with a homogeneous ground state) or that each ground state has a slightly different P_r* spectrum in this spectral region (with an inhomogeneous ground state). Small structural rearrangements are expected as the protein readjusts to the excited-state bilin

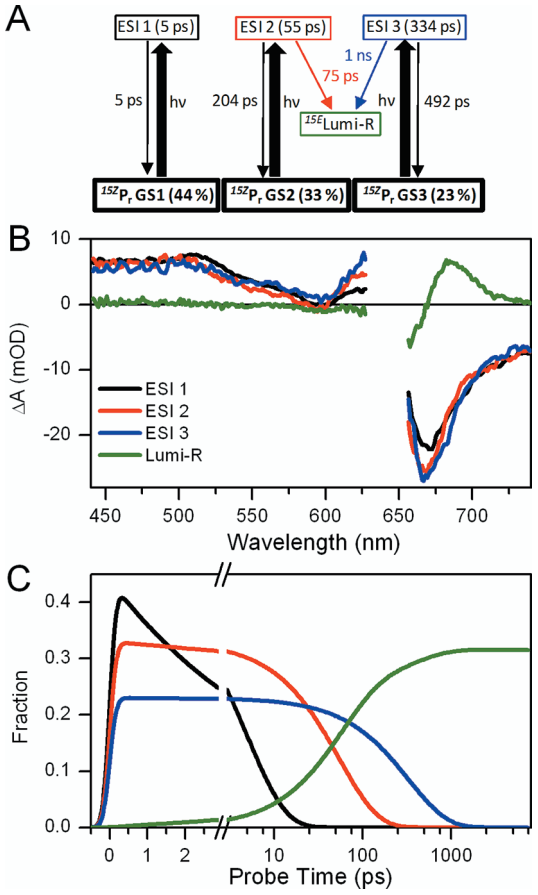

Figure 6. Global analysis of the forward reaction with three ground-state populations. (A) The target model has three P_r ground states, with occupancy levels indicated in parentheses. ESI1 does not generate Lumi-R. Time constants for each pathway are indicated, and the detailed photocycle yield is described in Table 1. (B) SADS based on the target model in panel A. (C) Concentration profile of each spectral species over time. The overall quantum yield of Lumi-R is 32%.

chromophore,[36] but it is also possible that ground-state inhomogeneity can be manifested in either varying kinetics or varying spectral features.

DISCUSSION

The high level of expression, good stability, and excellent switching efficiency of NpR6012g4 allowed us to undertake the first femtosecond characterization of any red/green CBCR, providing an interesting comparison to comparable studies on red/far-red phytochromes. This work also complements the characterization of the nanosecond-transient fluorescence of the red/green CBCR AnPixJ[26,30] by elucidating the primary photodynamics of the forward reaction ($^{15Z}P_r$ to $^{15E}P_g$). The complementary study of the primary photodynamics of the reverse ($^{15E}P_g$ to $^{15Z}P_r$) reaction of NpR6012g4 will be presented elsewhere.

Comparison of Red/Green and Red/Far-Red Photoreceptors. Red/green CBCRs such as AnPixJ, slr1393g2, and NpR6012g4 exhibit similarities to Cph1 and other red/far-red phytochromes, such as the similar $^{15Z}P_r$ ground state[9,26,52−56] and absorption spectra (Figure S4 of the Supporting Information). Of course, formation of a green-absorbing metastable state (P_g) rather than a far-red-absorbing state (P_{fr}) is an obvious difference. Moreover, if the lack of inversion of CD upon photoconversion in NpR6012g4 is representative, it means that the red/green CBCR photocycle is likely to produce the α-facial photoproduct observed with bacteriophytochromes utilizing biliverdin as a chromophore rather than the β-facial product observed with Cph1.[46]

In addition to similar $^{15Z}P_r$ ground states (Figure 7A), red/green CBCRs and red/far-red phytochromes give rise to very similar primary Lumi-R photoproducts (Figure 7B). The red-shifted Lumi-R formed in NpR6012g4 after excitation of the P_r state absorbs at 680 nm (Figure 3) and persists beyond the 7 ns range of the experiment. The SADS of both Lumi-G_1 and Lumi-G_2 exhibit photoproduct absorptions with magnitudes that are comparable to those of the respective bleaches.[39,40,57,58] Fukashima et al. recently explored the nanosecond to millisecond transient dynamics of AnPixJ and observed a similar appearance of a 680 nm Lumi-R absorption band before the 100 ns resolution of their experiment;[30] this species has largely decayed by 1 μs to form a subsequent intermediate. Red/far-red phytochrome systems such as Cph1 show a similar evolution of Lumi-R into a subsequent intermediate on a microsecond time scale.[59−63]

Spectrally, the ground-state absorptions of NpR6012g4 and Cph1 are nearly identical, with overlapping Soret bands and a minor ~10 nm red shift (~210 cm^{-1}) of the Cph1 red peak relative to that of NpR6012g4 (Figure 7A). Moreover, both NpR6012g4 and *Synechocystis* Cph1 also exhibit very similar observed kinetics for the decay of the respective P_r* excited-state populations (Figure 7C), although a wide range of multiphase decay kinetics has been reported for Lumi-R formation in red/far-red phytochromes. Holzwarth and co-workers found multiphasic decay of the excited state in the forward reaction for oat phytochrome A, arguing that only the 28 ps decay component generated Lumi-R.[39] Diller and co-workers analyzed Lumi-R formation in Cph1 as a distribution of rates, implying a heterogeneous P_r population.[40] In contrast, Mathies and co-workers used

Table 1. Model Parameters from Target Analysis[a]

population	initial occupancy (%)	$\tau_{effective}$	τ	partitioning	Lumi-R yield (%)
ESI1	44	5 ps	5 ps (GS1)	1.0 GS1	0
ESI2	33	55 ps	204 ps (GS2)	0.27 GS2	24
			75 ps (Lumi-R)	0.73 Lumi-R	
ESI3	23	334 ps	492 ps (GS3)	0.63 GS3	7.6
			1 ns (Lumi-R)	0.33 Lumi-R	
Lumi-R	0	∞	∞	N/A[b]	N/A[b]

[a]Initial occupancy is assumed to be equivalent to the relative levels of the three postulated ground states in the target model. Microscopic rate constants can be derived as the reciprocal of the relaxation time τ (with units of ps^{-1}). Partition factors are calculated from the relative decay times for ground-state regeneration and Lumi-R formation and reported as fractions. The total Lumi-R yield for each population is the product of the percentage of that population and the Lumi-R partition fraction for that population. [b]Not available.

dx.doi.org/10.1021/bi201507k | *Biochemistry* 2012, 51, 608−618

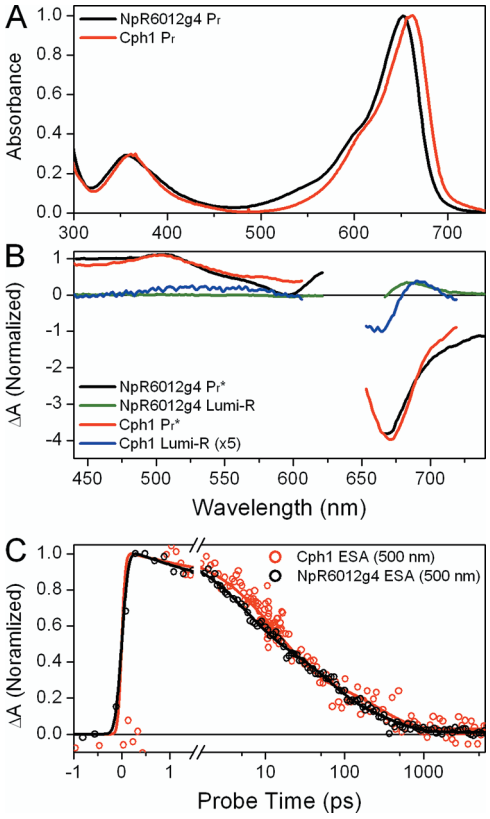

Figure 7. Comparison between NpR6012g4 and Cph1. (A) Comparison of the P_r ground-state absorption spectra. (B) Excited-state transient spectra and primary Lumi-R photoproduct SADS were normalized on the basis of the ESA band at ~500 nm. The good overlap on the bleach region validates the ESA band for normalization. The Lumi-R peak for Cph1 is scaled 5-fold to match the equivalent peak for NpR6012g4, indicating a greater quantum yield and/or Lumi-R extinction coefficient in NpR6012g4. (C) Kinetic traces of the ESA band (500 nm) for both proteins normalized by the maximum value and fitted with the global sequential model (solid line).

femtosecond stimulated Raman spectroscopy to measure 3 and 30 ps time constants for the formation of Lumi-R in Cph1,[38] but argued for a homogeneous mechanism to describe the nonexponential kinetics in their data.

The similarities in the static absorption spectra and transient excited-state decay kinetics in Cph1 and NpR6012g4 suggest the two proteins generate Lumi-R in a similar manner; however, this is incorrect. The 3 ps rapid decay component in Cph1 generates some Lumi-R,[37,38,43] which is quite different from the fast 5 ps time scale in NpR6012g4, in which no Lumi-R is generated (Figure 6A); only the two slower kinetic decay components with time constants of 75 ps and 1 ns generate Lumi-R (and very efficiently). Hence, NpR6012g4 is more similar to phytochromes RpBphP2 and RpBphP3 from *Rhodopseudomonas palustris*.[36] For RpBphP2, two fast excited-state kinetic components at 0.3 and 4.1 ps were attributed to deformation of the excited state, and Lumi-R formed only slowly with 220 ps and 1.9 ns time constants. RpBphP3, which is highly fluorescent and has an anomalous photocycle,[64] exhibits even slower formation of Lumi-R. It is thus possible that a correlation exists between slower Lumi-R formation and conservation of CD during the photocycle, perhaps indicating the presence of distinct classes of excited-state dynamics within the phytochrome superfamily.[32] This hypothesis will be tested as more ultrafast transient spectroscopic studies of CBCRs are completed.

Photoconversion of NpR6012g4. The ultrafast isomerization reactions of photoactive proteins such as rhodopsin and photoactive yellow protein (PYP) have been attributed to conical intersections in which the excited-state population is rapidly de-excited to the electronic ground state.[65,66] Direct evidence of the existence of such conical intersections in protein systems was first obtained only recently by using ultrafast near-IR probing to observe wavepacket dynamics.[67] For phytochromes, even theoretical evidence of conical intersections is lacking, partly because of the difficulties in conducting correlated excited-state calculations for systems as large as bilin chromophores. However, global analysis of the forward reaction of NpR6012g4 suggests the existence of a conical intersection. All transient spectra are composites of only P_r* and Lumi-R spectra (Figure 5D), without any structurally deformed metastable excited-state features. The absence of such features suggests that structurally deformed excited-state species exist only briefly on the excited-state potential energy surface. Hence, there is no current evidence of an excited-state photoproduct population in NpR6012g4, as has been proposed for Cph1.[38]

Figure 8 combines these aspects into simple two-dimensional PES diagrams of the productive reactions of NpR6012g4 (GS2

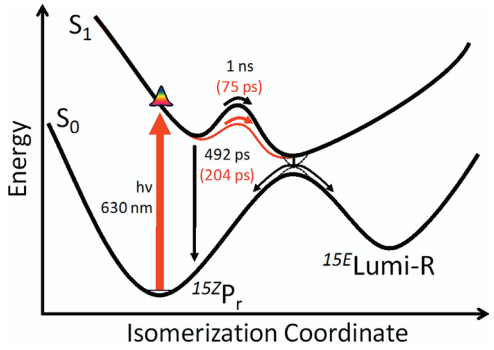

Figure 8. Potential energy surface diagram of NpR6012g4 initial forward photoreaction dynamics with respective time constants for the reaction. Only the ground states leading to Lumi-R are shown [GS2/ESI2 and GS3/ESI3 (Figure 6A)]. Time constants colored red describe the evolution of the faster ESI2 component. When the P_r ground state is excited to the first singlet excited state S^1, there is vibrational relaxation of the exited state to a local minimum, followed by partitioning over the excited-state barrier and rapid de-excitation to the fully isomerized Lumi-R ground state.

and GS3). We envision a conical intersection to explain the absence of excited-state photoproduct and an excited-state potential energy barrier to explain the slow isomerization relative to rhodopsin or PYP.[68,69] The multiple decay constants associated with Lumi-R formation are interpreted as different barrier heights on the excited-state surface for each P_r subpopulation. Such a barrier height could be modulated by protein environment such as hydrogen bonds and π-interactions;[36,70] thus, ground-state heterogeneity could give rise to populations with distinct excited-state barrier heights due to subtle structural heterogeneity giving rise to different protein−chromophore interactions. A more detailed mechanistic understanding of this photoreaction will benefit from structural data, time-resolved vibrational spectroscopy, and pump−dump−probe techniques, which are beyond the scope of these studies.

dx.doi.org/10.1021/bi201507k | *Biochemistry* 2012, 51, 608−618

Quantum Yield for the Forward Photocycle. A general correlation exists between excited-state lifetime and photocycle yields in photoreceptors, with systems that exhibit faster quenching kinetics also exhibiting an increased quantum yield (Φ). For example, rhodopsin has an ∼200 fs decay time with a Φ of ≈70%,[69] while PYP has a slower ∼2 ps quenching with a Φ of ≈30%[68] and Cph1 has an average 10 ps quenching with a Φ of ≈10−15%.[40] There are exceptions to this trend as well: El-Sayed and co-workers showed for bacteriorhodopsin that a 20-fold variation in reaction rate did not affect quantum yield,[62] and the reverse reaction of Cph1 has an estimated Φ (∼16%) comparable to that of the forward dynamics despite much faster excited-state decay.[63,64] However, a general correlation is observed in most studies. On the basis of this correlation, the similar kinetics for forward photoconversion of Cph1 and Npr6012g4 (Figure 7C) would imply comparable Φ values for the two proteins. Strikingly, however, the NpR6012g4 forward reaction exhibited a significantly higher Φ, estimated to be ∼32% in global analysis (Figure 6C). This measurement is not quantitative with the PP signals alone and has an innate uncertainty associated with it because the amplitude of the final Lumi-R spectra in the data is the product of the final population of Lumi-R (Φ) and its extinction (molar absorptivity). Hence, to fit the final Lumi-R signal amplitude, the scaling of one parameter requires the inverse scaling of the other parameter.[34]

Quantifying absolute Φ is difficult and requires precise measurement of both the number of chromophores initially excited at early times and the number of chromophores converted to the photoproduct at late times. This can be derived from transient absorbance data if there is a clean bleach region in the spectrum, undisturbed by overlapping ESA, SE, or photoproduct absorptions, which is true in PYP.[41,71,72] Unfortunately, such a clean bleach does not exist in either the P_r* or Lumi-R spectra of NpR6012g4 (Figure 3). Kennis and co-workers recently estimated the Φ values for RpBphP2 and RpBphP3 to be 13 and 6%, respectively, by comparing the initial and final amplitudes of the vibronic bleach band at 635−640 nm[36] with a ground-state absorbance at longer wavelengths due to the structural differences between biliverdin and PCB chromophores.[5,12] However, the equivalent region of the spectrum for NpR6012g4 is strongly overlapped by the broad ESA band (Figure 3) such that the initial excited-state signal has a positive amplitude between those two bleach bands, thus making such an analysis ill-suited here.

Despite this limitation, an approximate estimation of the Φ is possible in NpR6012g4 by using Cph1 as a reference. Although Cph1 and NpR6012g4 suffer from similar overlaps in the transient signals (Figure 7B), Cph1 has an independently measured Φ of 10−15%[38,44] and is similar to that of plant phytochrome.[73] We therefore normalized the transient spectral data set (at all probe times, including the final photoproduct spectra for NpR6012g4 and Cph1) to the initial amplitude of the ESA band at ∼500 nm (Figure 7B). This scaling also normalizes the bleach region for the two proteins as expected because of the strong spectral and temporal similarities between the two proteins. Strikingly, the magnitude of the final Lumi-R spectrum (Figure 7B, green curve) after this normalization is 5-fold greater in NpR6012g4 than in Cph1 (Figure 7B, blue curve). If the two Lumi-R populations, with their nearly identical spectral features, exhibit comparable extinction coefficients (and the ESA and bleach bands), then Φ for NpR6012g4 must be 5-fold greater than for Cph1. Alternately, if Φ is identical for the two proteins, then the Lumi-R extinction coefficient would have to be 5-fold higher.

For the $^{15Z}P_r$ ground state, Cph1 and NpR6012g4 have comparable extinction coefficients with 85000 M^{-1} cm^{-1} for Cph1[74] and 98000 M^{-1} cm^{-1} for NpR6012g4 based on our denaturation data and published values for acid-denatured bilin chromophores.[75] Although the extinction coefficient of Lumi-R is unknown, a difference as great as 5-fold seems highly unlikely; similarly, a 5-fold enhancement of Φ relative to that of Cph1 would imply a Φ of 50−75%, which seems very high for such a slow relaxation process. Therefore, the quantum yield of NpR6012g4's forward reaction is likely to be somewhat greater than that of Cph1, and the Lumi-R photoproduct is also likely to have a greater extinction coefficient. The calculated quantum yield of 32% from the target model is intended as a reasonable compromise (Figure 6C). A more accurate estimate of the Lumi-R quantum yield can be obtained with femtosecond pump−dump−probe measurements that provide additional constraints for the data analysis. Such an analysis supports a comparable estimate for Φ of 40%.[76] The forward reaction of red/green CBCRs thus has dynamics similar to that of the equivalent reaction in red/far-red phytochromes but exhibits a significantly higher quantum yield. The observation of such a high quantum yield also implies potential for improving Φ in red/far-red systems, which would provide an informative contrast to successful attempts to increase the nonproductive fluorescence quantum yield in such systems.[7,27,29,36,70,77] Were the design principles for such super-efficient phytochromes to prove to be general, one could envision the use of such alleles in plants to trigger phytochrome-regulated developmental control at lower excitation fluences. Moreover, our observation of an inactive population in NpR6012g4 provides a possible explanation for closely related but photoinactive proteins:[26] such proteins may simply partition most or all of the total ground state into such inactive populations.

■ CONCLUDING COMMENTS

We present the first femtosecond study of the primary dynamics underlying the forward switching (red to green) in the new cyanobacteriochrome (CBCR) class of phytochrome proteins. The NpR6012g4 GAF domain exhibits photoswitching capacity without requiring either PHY or PAS domains commonly required in red/far red phytochromes. The spectral absorption and transient kinetics after excitation of P_r (including multiphasic excited-state kinetics) are remarkably similar to those of the cyanobacterial Cph1 from *Synechocystis*. To separate the apparent (observed) kinetics into microscopic kinetics, the data are modeled within an inhomogeneous multicompartment (population) model. This model postulates each decay time scale of P_r* is attributed to a separate ground-state P_r population with different excited-state barriers (and hence excited-state kinetics) for PCB isomerization and formation of Lumi-R. In contrast to Cph1 and other red/far-red phytochromes, the fastest phase (5 ps) does not form Lumi-R, the primary photoproduct, in any appreciable amount. Although the excited-state time scales are similar for Cph1 and NpR6012g4, the yield of Lumi-R is 2- or 3-fold larger, indicating that different mechanisms are at play in the initiation dynamics of this red/green CBCR.

■ ASSOCIATED CONTENT

Supporting Information

Four figures. This material is available free of charge via the Internet at http://pubs.acs.org.

AUTHOR INFORMATION

Corresponding Author

*Department of Chemistry, University of California, Davis, CA 95616. Telephone: (530) 754-9075. E-mail: dlarsen@ucdavis.edu.

Funding

This work was supported by a grant from the Chemical Sciences, Geosciences, and Biosciences Division, Office of Basic Energy Sciences, Office of Science, U.S. Department of Energy (DOE DE-FG02-09ER16117), to both J.C.L. and D.S.L.

ACKNOWLEDGMENTS

We thank Elsie L. Campbell and Prof. Jack Meeks (University of California, Davis, CA) for the generous gift of *N. punctiforme* genomic DNA and Lu Zhao for help with data collection.

ABBREVIATIONS

CBCR, cyanobacteriochrome; CBD, chitin-binding domain; CD, circular dichroism; EADS, evolution-associated difference spectra; SADS, species-associated difference spectra; ESI, excited-state intermediate; ESA, excited-state absorption; SE, stimulated emission; GAF, domain name derived from cGMP phosphodiesterase/adenylyl cyclase/FhlA; GSA, ground-state absorbance; NOPA, noncollinear optical parametric amplifier; PAS, domain name derived from the *Drosophila* period clock, mammalian aromatic hydrocarbon nuclear transporter, and *Drosophila* single-minded proteins; PCB, phycocyanobilin; P_r, red-absorbing ground state of red/far-red phytochromes; P_{fr}, far-red-absorbing photoproduct state of red/far-red phytochromes; $^{15Z}P_r$, red-absorbing ground state of red/green CBCRs; $^{15E}P_g$, green-absorbing photoproduct state of red/green CBCRs; Pr*, excited-state population(s) derived from photoexcitation of P_r or $^{15Z}P_r$; PYP, photoactive yellow protein; Φ, photocycle quantum yield.

REFERENCES

(1) Rockwell, N. C., Su, Y. S., and Lagarias, J. C. (2006) Phytochrome structure and signaling mechanisms. *Annu. Rev. Plant Biol. 57*, 837−858.

(2) van der Horst, M. A., Key, J., and Hellingwerf, K. J. (2007) Photosensing in chemotrophic, non-phototrophic bacteria: Let there be light sensing too. *Trends Microbiol. 15*, 554−562.

(3) Hirose, Y., Narikawa, R., Katayama, M., and Ikeuchi, M. (2010) Cyanobacteriochrome CcaS regulates phycoerythrin accumulation in *Nostoc punctiforme*, a group II chromatic adapter. *Proc. Natl. Acad. Sci. U.S.A. 107*, 8854−8859.

(4) Möglich, A., Yang, X., Ayers, R. A., and Moffat, K. (2010) Structure and Function of Plant Photoreceptors. *Annu. Rev. Plant Biol. 61*, 21−47.

(5) Auldridge, M. E., and Forest, K. T. (2011) Bacterial phytochromes: More than meets the light. *Crit. Rev. Biochem. Mol. Biol. 46*, 67−88.

(6) Levskaya, A., Weiner, O. D., Lim, W. A., and Voigt, C. A. (2009) Spatiotemporal control of cell signalling using a light-switchable protein interaction. *Nature 461*, 997−1001.

(7) Shu, X. K., Royant, A., Lin, M. Z., Aguilera, T. A., Lev-Ram, V., Steinbach, P. A., and Tsien, R. Y. (2009) Mammalian Expression of Infrared Fluorescent Proteins Engineered from a Bacterial Phytochrome. *Science 324*, 804−807.

(8) Möglich, A., and Moffat, K. (2010) Engineered photoreceptors as novel optogenetic tools. *Photochem. Photobiol. Sci. 9*, 1286−1300.

(9) Zhang, J. A., Wu, X. J., Wang, Z. B., Chen, Y., Wang, X., Zhou, M., Scheer, H., and Zhao, K. H. (2010) Fused-Gene Approach to Photoswitchable and Fluorescent Biliproteins. *Angew. Chem., Int. Ed. 49*, 5456−5458.

(10) Drepper, T., Krauss, U., Berstenhorst, S. M. Z., Pietruszka, J., and Jaeger, K. E. (2011) Lights on and action! Controlling microbial gene expression by light. *Appl. Microbiol. Biotechnol. 90*, 23−40.

(11) Rana, A., and Dolmetsch, R. E. (2010) Using light to control signaling cascades in live neurons. *Curr. Opin. Neurobiol. 20*, 617−622.

(12) Rockwell, N. C., and Lagarias, J. C. (2010) A Brief History of Phytochromes. *ChemPhysChem 11*, 1172−1180.

(13) Rohmer, T., Lang, C., Gartner, W., Hughes, J., and Matysik, J. (2010) Role of the Protein Cavity in Phytochrome Chromoprotein Assembly and Double-bond Isomerization: A Comparison with Model Compounds. *Photochem. Photobiol. 86*, 856−861.

(14) Song, C., Psakis, G., Lang, C., Mailliet, J., Gartner, W., Hughes, J., and Matysik, J. (2011) Two ground state isoforms and a chromophore D-ring photoflip triggering extensive intramolecular changes in a canonical phytochrome. *Proc. Natl. Acad. Sci. U.S.A. 108*, 3842−3847.

(15) Wagner, J. R., Brunzelle, J. S., Forest, K. T., and Vierstra, R. D. (2005) A light-sensing knot revealed by the structure of the chromophore-binding domain of phytochrome. *Nature 438*, 325−331.

(16) Wagner, J. R., Zhang, J. R., Brunzelle, J. S., Vierstra, R. D., and Forest, K. T. (2007) High resolution structure of *Deinococcus* bacteriophytochrome yields new insights into phytochrome architecture and evolution. *J. Biol. Chem. 282*, 12298−12309.

(17) Xiaojing, Y., Stojkovic, E. A., Kuk, J., and Moffat, K. (2007) Crystal structure of the chromophore binding domain of an unusual bacteriophytochrome, RpBphP3, reveals residues that modulate photoconversion. *Proc. Natl. Acad. Sci. U.S.A. 104*, 12571−12576.

(18) Essen, L. O., Mailliet, J., and Hughes, J. (2008) The structure of a complete phytochrome sensory module in the Pr ground state. *Proc. Natl. Acad. Sci. U.S.A. 105*, 14709−14714.

(19) Yang, X., Kuk, J., and Moffat, K. (2008) Crystal structure of *Pseudomonas aeruginosa* bacteriophytochrome: Photoconversion and signal transduction. *Proc. Natl. Acad. Sci. U.S.A. 105*, 14715−14720.

(20) Wu, S. H., and Lagarias, J. C. (2000) Defining the bilin lyase domain: Lessons from the extended phytochrome superfamily. *Biochemistry 39*, 13487−13495.

(21) Ikeuchi, M., and Ishizuka, T. (2008) Cyanobacteriochromes: A new superfamily of tetrapyrrole-binding photoreceptors in cyanobacteria. *Photochem. Photobiol. Sci. 7*, 1159−1167.

(22) Yoshihara, S., Katayama, M., Geng, X. X., and Ikeuchi, M. (2004) Cyanobacterial phytochrome-like PixJ1 holoprotein shows novel reversible photoconversion between blue- and green-absorbing forms. *Plant Cell Physiol. 45*, 1729−1737.

(23) Ishizuka, T., Shimada, T., Okajima, K., Yoshihara, S., Ochiai, Y., Katayama, M., and Ikeuchi, M. (2006) Characterization of cyanobacteriochrome TePixJ from a thermophilic cyanobacterium *Thermosynechococcus elongatus* strain BP-1. *Plant Cell Physiol. 47*, 1251−1261.

(24) Ishizuka, T., Narikawa, R., Kohchi, T., Katayama, M., and Ikeuchi, M. (2007) Cyanobacteriochrome TePixJ of *Thermosynechococcus elongatus* harbors phycoviolobilin as a chromophore. *Plant Cell Physiol. 48*, 1385−1390.

(25) Hirose, Y., Shimada, T., Narikawa, R., Katayama, M., and Ikeuchi, M. (2008) Cyanobacteriochrome CcaS is the green light receptor that induces the expression of phycobilisome linker protein. *Proc. Natl. Acad. Sci. U.S.A. 105*, 9528−9533.

(26) Narikawa, R., Fukushima, Y., Ishizuka, T., Itoh, S., and Ikeuchi, M. (2008) A novel photoactive GAF domain of cyanobacteriochrome AnPixJ that shows reversible green/red photoconversion. *J. Mol. Biol. 380*, 844−855.

(27) Rockwell, N. C., Njuguna, S. L., Roberts, L., Castillo, E., Parson, V. L., Dwojak, S., Lagarias, J. C., and Spiller, S. C. (2008) A second conserved GAF domain cysteine is required for the blue/green photoreversibility of cyanobacteriochrome Tlr0924 from *Thermosynechococcus elongatus*. *Biochemistry 47*, 7304−7316.

(28) Narikawa, R., Muraki, N., Shiba, T., Ikeuchi, M., and Kurisu, G. (2009) Crystallization and preliminary X-ray studies of the chromophore-binding domain of cyanobacteriochrome AnPixJ from *Anabaena* sp. PCC 7120. *Acta Crystallogr. F65*, 159−162.

(29) Ulijasz, A. T., Cornilescu, G., von Stetten, D., Cornilescu, C., Escobar, F. V., Zhang, J., Stankey, R. J., Rivera, M., Hildebrandt, P., and Vierstra, R. D. (2009) Cyanochromes Are Blue/Green Light Photoreversible Photoreceptors Defined by a Stable Double Cysteine Linkage to a Phycoviolobilin-type Chromophore. *J. Biol. Chem. 284*, 29757−29772.
(30) Fukushima, Y., Iwaki, M., Narikawa, R., Ikeuchi, M., Tomita, Y., and Itoh, S. (2011) Photoconversion Mechanism of a Green/Red Photosensory Cyanobacteriochrome AnPixJ: Time-Resolved Optical Spectroscopy and FTIR Analysis of the AnPixJ-GAF2 Domain. *Biochemistry 50*, 6328−6339.
(31) Ishizuka, T., Kamiya, A., Suzuki, H., Narikawa, R., Noguchi, T., Kohchi, T., Inomata, K., and Ikeuchi, M. (2011) The Cyanobacteriochrome, TePixJ, Isomerizes Its Own Chromophore by Converting Phycocyanobilin to Phycoviolobilin. *Biochemistry 50*, 953−961.
(32) Rockwell, N. C., Martin, S. S., Feoktistova, K., and Lagarias, J. C. (2011) Diverse two-cysteine photocycles in phytochromes and cyanobacteriochromes. *Proc. Natl. Acad. Sci. U.S.A. 108*, 11854−11859.
(33) Song, J. Y., Cho, H. S., Cho, J. I., Jeon, J. S., Lagarias, J. C., and Park, Y. I. (2011) Near-UV cyanobacteriochrome signaling system elicits negative phototaxis in the cyanobacterium *Synechocystis* sp. PCC 6803. *Proc. Natl. Acad. Sci. U.S.A. 108*, 10780−10785.
(34) van Stokkum, I. H. M., Larsen, D. S., and van Grondelle, R. (2004) Global and target analysis of time-resolved spectra. *Biochim. Biophys. Acta 1657*, 82−104.
(35) Holzwarth, A. R. (1996) Data Analysis of Time-Resolved Measurements. In *Biophysical techniques in photosynthesis* (Amesz, J., and Hoff, A. J., Eds.) pp 75−92, Springer, Dordrecht, The Netherlands.
(36) Toh, K. C., Stojkovic, E. A., van Stokkum, I. H. M., Moffat, K., and Kennis, J. T. M. (2010) Proton-transfer and hydrogen-bond interactions determine fluorescence quantum yield and photochemical efficiency of bacteriophytochrome. *Proc. Natl. Acad. Sci. U.S.A. 107*, 9170−9175.
(37) van Wilderen, L., Clark, I. P., Towrie, M., and van Thor, J. J. (2009) Mid-Infrared Picosecond Pump-Dump-Probe and Pump-Repump-Probe Experiments to Resolve a Ground-State Intermediate in Cyanobacterial Phytochrome Cph1. *J. Phys. Chem. B 113*, 16354−16364.
(38) Dasgupta, J., Frontiera, R. R., Taylor, K. C., Lagarias, J. C., and Mathies, R. A. (2009) Ultrafast excited-state isomerization in phytochrome revealed by femtosecond stimulated Raman spectroscopy. *Proc. Natl. Acad. Sci. U.S.A. 106*, 1784−1789.
(39) Müller, M. G., Lindner, I., Martin, I., Gartner, W., and Holzwarth, A. R. (2008) Femtosecond kinetics of photoconversion of the higher plant photoreceptor phytochrome carrying native and modified chromophores. *Biophys. J. 94*, 4370−4382.
(40) Heyne, K., Herbst, J., Stehlik, D., Esteban, B., Lamparter, T., Hughes, J., and Diller, R. (2002) Ultrafast dynamics of phytochrome from the cyanobacterium *Synechocystis*, reconstituted with phycocyanobilin and phycoerythrobilin. *Biophys. J. 82*, 1004−1016.
(41) Larsen, D. S., van Stokkum, I. H. M., Vengris, M., van der Horst, M. A., de Weerd, F. L., Hellingwerf, K. J., and van Grondelle, R. (2004) Incoherent manipulation of the photoactive yellow protein photocycle with dispersed pump-dump-probe spectroscopy. *Biophys. J. 87*, 1858−1872.
(42) Kennis, J. T. M., Larsen, D. S., van Stokkum, I. H. M., Vengris, M., van Thor, J. J., and van Grondelle, R. (2004) Uncovering the hidden ground state of green fluorescent protein. *Biophys. J. 86*, 168A.
(43) van Thor, J. J., Ronayne, K. L., and Towrie, M. (2007) Formation of the early photoproduct Lumi-R of cyanobacterial phytochrome Cph1 observed by ultrafast mid-infrared spectroscopy. *J. Am. Chem. Soc. 129*, 126−132.
(44) Lamparter, T., Mittmann, F., Gartner, W., Borner, T., Hartmann, E., and Hughes, J. (1997) Characterization of recombinant phytochrome from the cyanobacterium *Synechocystis*. *Proc. Natl. Acad. Sci. U.S.A. 94*, 11792−11797.
(45) Edgar, R. C. (2004) MUSCLE: Multiple sequence alignment with high accuracy and high throughput. *Nucleic Acids Res. 32*, 1792−1797.
(46) Rockwell, N. C., Shang, L., Martin, S. S., and Lagarias, J. C. (2009) Distinct classes of red/far-red photochemistry within the phytochrome superfamily. *Proc. Natl. Acad. Sci. U.S.A. 106*, 6123−6127.
(47) Gambetta, G. A., and Lagarias, J. C. (2001) Genetic engineering of phytochrome biosynthesis in bacteria. *Proc. Natl. Acad. Sci. U.S.A. 98*, 10566−10571.
(48) Shang, L., Rockwell, N. C., Martin, S. S., and Lagarias, J. C. (2010) Biliverdin Amides Reveal Roles for Propionate Side Chains in Bilin Reductase Recognition and in Holophytochrome Assembly and Photoconversion. *Biochemistry 49*, 6070−6082.
(49) Carroll, E. C., Compton, O. C., Madsen, D., Osterloh, F. E., and Larsen, D. S. (2008) Ultrafast carrier dynamics in exfoliated and functionalized calcium niobate nanosheets in water and methanol. *J. Phys. Chem. C 112*, 2394−2403.
(50) Seibeck, S., Borucki, B., Otto, H., Inomata, K., Khawn, H., Kinoshita, H., Michael, N., Lamparter, T., and Heyn, M. P. (2007) Locked 5Zs-biliverdin blocks the Meta-R-A to Meta-R-C transition in the functional cycle of bacteriophytochrome Agp1. *FEBS Lett. 581*, 5425−5429.
(51) Spillane, K. M., Dasgupta, J., Lagarias, J. C., and Mathies, R. A. (2009) Homogeneity of Phytochrome Cph1 Vibronic Absorption Revealed by Resonance Raman Intensity Analysis. *J. Am. Chem. Soc. 131*, 13946−13948.
(52) Hughes, J., Lamparter, T., Mittmann, F., Hartmann, E., Gartner, W., Wilde, A., and Borner, T. (1997) A prokaryotic phytochrome. *Nature 386*, 663−663.
(53) Yeh, K. C., Wu, S. H., Murphy, J. T., and Lagarias, J. C. (1997) A cyanobacterial phytochrome two-component light sensory system. *Science 277*, 1505−1508.
(54) Davis, S. J., Vener, A. V., and Vierstra, R. D. (1999) Bacteriophytochromes: Phytochrome-like photoreceptors from nonphotosynthetic eubacteria. *Science 286*, 2517−2520.
(55) Giraud, E., Fardoux, L., Fourrier, N., Hannibal, L., Genty, B., Bouyer, P., Dreyfus, B., and Vermeglio, A. (2002) Bacteriophytochrome controls photosystem synthesis in anoxygenic bacteria. *Nature 417*, 202−205.
(56) Noack, S., Michael, N., Rosen, R., and Lamparter, T. (2007) Protein conformational changes of *Agrobacterium* phytochrome Agp1 during chromophore assembly and photoconversion. *Biochemistry 46*, 4164−4176.
(57) Rentsch, S., Hermann, G., Bischoff, M., Strehlow, D., and Rentsch, M. (1997) Femtosecond spectroscopic studies on the red light-absorbing form of oat phytochrome and 2,3-dihydrobiliverdin. *Photochem. Photobiol. 66*, 585−590.
(58) Bischoff, M., Hermann, G., Rentsch, S., and Strehlow, D. (2001) First steps in the phytochrome phototransformation: A comparative femtosecond study on the forward (Pr → Pfr) and back reaction (Pfr → Pr). *Biochemistry 40*, 181−186.
(59) Remberg, A., Lindner, I., Lamparter, T., Hughes, J., Kneip, C., Hildebrandt, P., Braslavsky, S. E., Gartner, W., and Schaffner, K. (1997) Raman spectroscopic and light-induced kinetic characterization of a recombinant phytochrome of the cyanobacterium *Synechocystis*. *Biochemistry 36*, 13389−13395.
(60) van Thor, J. J., Borucki, B., Crielaard, W., Otto, H., Lamparter, T., Hughes, J., Hellingwerf, K. J., and Heyn, M. P. (2001) Light-induced proton release and proton uptake reactions in the cyanobacterial phytochrome Cph1. *Biochemistry 40*, 11460−11471.
(61) Scurlock, R. D., Evans, C. H., Braslavsky, S. E., and Schaffner, K. (1993) A Phytochrome Phototransformation Study Using 2-Laser 2-Color Flash-Photolysis: Analysis of the Decay Mechanism of I(700). *Photochem. Photobiol. 58*, 106−115.
(62) Song, L., El−Sayed, M. A., and Lanyi, J. K. (1993) Protein Catalysis of the Retinal Subpicosecond Photoisomerization in the Primary Process of Bacteriorhodopsin Photosynthesis. *Science 261*, 891−894.
(63) Lamparter, T., Mittmann, F., Gartner, W., Borner, T., Hartmann, E., and Hughes, J. (1997) Characterization of recombinant phytochrome from the cyanobacterium Synechocystis.

Proceedings of the National Academy of Sciences of the United States of America 94, 11792−11797.
(64) Heyne, K., Herbst, J., Stehlik, D., Esteban, B., Lamparter, T., Hughes, J., and Diller, R. (2002) Ultrafast dynamics of phytochrome from the cyanobacterium Synechocystis, reconstituted with phycocyanobilin and phycoerythrobilin. *Biophys. J. 82*, 1004−1016.
(65) Zhang, C. F., Farrens, D. L., Bjorling, S. C., Song, P. S., and Kliger, D. S. (1992) Time-Resolved Absorption Studies of Native Etiolated Oat Phytochrome. *J. Am. Chem. Soc. 114*, 4569−4580.
(66) Schmidt, P., Westphal, U. H., Worm, K., Braslavsky, S. E., Gartner, W., and Schaffner, K. (1996) Chromophore-protein interaction controls the complexity of the phytochrome photocycle. *J. Photochem. Photobiol., B 34*, 73−77.
(67) Giraud, E., Zappa, S., Vuillet, L., Adriano, J. M., Hannibal, L., Fardoux, J., Berthomieu, C., Bouyer, P., Pignol, D., and Vermeglio, A. (2005) A new type of bacteriophytochrome acts in tandem with a classical bacteriophytochrome to control the antennae synthesis in *Rhodopseudomonas palustris*. *J. Biol. Chem. 280*, 32389−32397.
(68) Levine, B. G., and Martinez, T. J. (2007) Isomerization through conical intersections. *Annu. Rev. Phys. Chem. 58*, 613−634.
(69) Schapiro, I., Ryazantsev, M. N., Frutos, L. M., Ferre, N., Lindh, R., and Olivucci, M. (2011) The ultrafast photoisomerizations of rhodopsin and bathorhodopsin are modulated by bond length alternation and HOOP driven electronic effects. *J. Am. Chem. Soc. 133*, 3354−3364.
(70) Polli, D., Altoe, P., Weingart, O., Spillane, K. M., Manzoni, C., Brida, D., Tomasello, G., Orlandi, G., Kukura, P., Mathies, R. A., Garavelli, M., and Cerullo, G. (2010) Conical intersection dynamics of the primary photoisomerization event in vision. *Nature 467*, 440−488.
(71) Vanbrederode, M. E., Gensch, T., Hoff, W. D., Hellingwerf, K. J., and Braslavsky, S. E. (1995) Photoinduced Volume Change and Energy-Storage Associated with the Early Transformations of the Photoactive Yellow Protein from *Ectothiorhodospira halophila*. *Biophys. J. 68*, 1101−1109.
(72) Kim, J. E., Tauber, M. J., and Mathies, R. A. (2001) Wavelength dependent cis-trans isomerization in vision. *Biochemistry 40*, 13774−13778.
(73) Fischer, A. J., and Lagarias, J. C. (2004) Harnessing phytochrome's glowing potential. *Proc. Natl. Acad. Sci. U.S.A. 101*, 17334−17339.
(74) Carroll, E. C., Song, S.-H., Kumauchi, M., van Stokkum, I. H. M., Jailaubekov, A., Hoff, W. D., and Larsen, D. S. (2010) Subpicosecond Excited-State Proton Transfer Preceding Isomerization During the Photorecovery of Photoactive Yellow Protein. *J. Phys. Chem. Lett. 1*, 2793−2799.
(75) Carroll, E. C., Hospes, M., Valladares, C., Hellingwerf, K. J., and Larsen, D. S. (2011) Is the photoactive yellow protein a UV-B/blue light photoreceptor? *Photochem. Photobiol. Sci. 10*, 464−468.
(76) Kelly, J. M., and Lagarias, J. C. (1985) Photochemistry of 124-Kilodalton Avena Phytochrome under Constant Illumination in vitro. *Biochemistry 24*, 6003−6010.
(77) Lamparter, T., Esteban, B., and Hughes, J. (2001) Phytochrome Cph1 from the cyanobacterium *Synechocystis* PCC6803: Purification, assembly, and quaternary structure. *Eur. J. Biochem. 268*, 4720−4730.
(78) Blot, N., Wu, X. J., Thomas, J. C., Zhang, J., Garczarek, L., Bohm, S., Tu, J. M., Zhou, M., Ploscher, M., Eichacker, L., Partensky, F., Scheer, H., and Zhao, K. H. (2009) Phycourobilin in trichromatic phycocyanin from oceanic cyanobacteria is formed post-translationally by a phycoerythrobilin lyase-isomerase. *J. Biol. Chem. 284*, 9290−9298.
(79) Kim, P. W., Freer, L. H., Rockwell, N. C., Martin, S. S., Lagarias, J. C., and Larsen, D. S. (2012) Second-Chance Initiation Dynamics of the Cyanobacterial Photocycle in the NpR6012 GAF 4 Domain of *Nostoc punctiforme*. *J. Am. Chem. Soc. 134*, DOI:10.1021/ja209533x.
(80) Fischer, A. J., Rockwell, N. C., Jang, A. Y., Ernst, L. A., Waggoner, A. S., Duan, Y., Lei, H. X., and Lagarias, J. C. (2005) Multiple roles of a conserved GAF domain tyrosine residue in cyanobacterial and plant phytochromes. *Biochemistry 44*, 15203−15215.